



# CHORUS

This is the accepted manuscript made available via CHORUS. The article has been published as:

## Vectorlike leptons: Muon $g-2$ anomaly, lepton flavor violation, Higgs boson decays, and lepton nonuniversality

Zijie Poh and Stuart Raby

Phys. Rev. D **96**, 015032 — Published 26 July 2017

DOI: [10.1103/PhysRevD.96.015032](https://doi.org/10.1103/PhysRevD.96.015032)

# Vector-like Leptons: Muon $g-2$ Anomaly, Lepton Flavor Violation, Higgs Decays, and Lepton Non-Universality

Zijie Poh<sup>1\*</sup> and Stuart Raby<sup>1†</sup>

<sup>1</sup>*Department of Physics*

*The Ohio State University*

*191 W. Woodruff Ave, Columbus, OH 43210, USA*

## Abstract

In this paper, we consider the Standard Model (SM) with one family of vector-like (VL) leptons, which couple to all three families of the SM leptons. We study the constraints on this model coming from the heavy charged lepton mass bound, electroweak precision data, the muon anomalous magnetic moment, lepton flavor violation, Higgs decay constraints, and a recently measured lepton non-universality observable,  $R_{K^{*0}}$ , along with  $R_K$ . We find that the strongest constraints are coming from the muon  $g-2$ ,  $R_{\mu\mu} = \Gamma(h \rightarrow \mu\mu)/\Gamma(h \rightarrow \mu\mu)_{\text{SM}}$ ,  $R_{\gamma\gamma}$  and  $\text{BR}(\mu \rightarrow e\gamma)$ . Although VL leptons couple to all three families of the SM leptons, the ratio of electron-VL to muon-VL coupling is constrained to be  $\langle \lambda_e/\lambda_\mu \rangle \lesssim 10^{-4}$ . We also find that this model cannot fit the lepton non-universality discrepancies.

---

\*poh.7@osu.edu

†raby.1@osu.edu

# 1 INTRODUCTION

The Standard Model (SM) is a highly successful theory in predicting and fitting many experimental measurements, with few exceptions. One of the discrepancies between the SM prediction and experimental measurement that has been known for a long time, is the muon anomalous magnetic moment. The experimentally measured muon anomalous magnetic moment and the SM prediction are given by [1]

$$\begin{aligned} a_\mu^{\text{exp}} &= 11659209.1(5.4)(3.3) \times 10^{-10}, \\ a_\mu^{\text{SM}} &= 11659180.3(0.1)(4.2)(2.6) \times 10^{-10}. \end{aligned} \quad (1)$$

The discrepancy between the experimental and theoretical values is [1]

$$\Delta a_\mu = a_\mu^{\text{exp}} - a_\mu^{\text{SM}} = 288(63)(49) \times 10^{-11}. \quad (2)$$

A simple extension of the SM that is able to explain this discrepancy is the SM with one family of VL leptons. Dermíšek et. al. showed that such a model with VL leptons coupling exclusively to the muon is sufficient to explain this discrepancy [2]. In a more natural theory, however, the VL leptons would couple to all three families of the SM leptons, which have been studied extensively in the literature [3–6]. Due to the lepton flavor violating nature of this model, the SM-VL couplings are known to be highly constrained.

In this paper, we try to provide a holistic point of view of the model in which the SM is extended by one family of VL leptons and the VL leptons have non-zero couplings to all three families of the SM leptons. We are interested in the constraints on this model coming from satisfying the heavy charged lepton mass bound, electroweak precision data, the muon  $g - 2$ , lepton flavor violation (LFV), Higgs decay constraints, and a recently measured lepton non-universality observable,  $R_{K^{*0}}$ , along with  $R_K$ . We find that this model cannot simultaneously satisfy electroweak precision measurements and the lepton non-universality discrepancies. As for the other observables, we find that the most constraining observables are the muon  $g - 2$ ,  $R_{\mu\mu} = \Gamma(h \rightarrow \mu\mu)/\Gamma(h \rightarrow \mu\mu)_{\text{SM}}$ ,  $R_{\gamma\gamma}$  and  $\text{BR}(\mu \rightarrow e\gamma)$ .

## 2 MODEL

The model that we study is the SM with one generation of VL leptons. The particles in the leptonic sector and their corresponding quantum numbers are given in Table 1 and the leptonic sector Lagrangian is given by

$$\begin{aligned} \mathcal{L} \supset & - \bar{\ell}_{Li} y_{ii}^e e_{Ri} H - \bar{\ell}_{Li} \lambda_i^E E_R H - \bar{L}_L \lambda_i^L e_{Ri} H - \bar{L}_L \lambda E_R H - \bar{E}_L \bar{\lambda} L_R H^\dagger \\ & - M_L \bar{L}_L L_R - M_E \bar{E}_L E_R + \text{h.c.}, \end{aligned} \quad (3)$$

where  $i = 1, 2, 3$  is the SM family index.

	SM			VL	
	$\ell_{Li} = \begin{pmatrix} \nu_{Li} \\ e_{Li} \end{pmatrix}$	$e_{Ri}$	$H = \begin{pmatrix} \phi^+ \\ v + (h + i\phi^0)/\sqrt{2} \end{pmatrix}$	$L_{L,R} = \begin{pmatrix} L_{L,R}^0 \\ L_{L,R}^- \end{pmatrix}$	$E_{L,R}$
$SU(2)_L$	2	1	2	2	1
$U(1)_Y$	-1	-2	1	-1	-2

Table 1: The quantum numbers of leptonic sector particles.  $i = 1, 2, 3$  is SM family index. The electric charge is given by  $Q = T_3 + Y/2$  and the Higgs vacuum expectation value is 174 GeV. The fields  $h, \phi^+$ , and  $\phi^0$  are the physical Higgs boson and the would-be Nambu-Goldstone bosons, respectively, which give the  $W^\pm$  boson and  $Z$  boson mass.

### Lepton Mass Matrix

Without loss of generality, we assume that the SM lepton Yukawa matrix,  $y^e$ , is already diagonalized. Thus, the lepton mass matrix is

$$\begin{pmatrix} \bar{e}_{Li} & \bar{L}_L^- & \bar{E}_L \end{pmatrix} \begin{pmatrix} y_{ii}^e v & 0 & \lambda_i^E v \\ \lambda_i^L v & M_L & \lambda v \\ 0 & \bar{\lambda} v & M_E \end{pmatrix} \begin{pmatrix} e_{Ri} \\ L_R^- \\ E_R \end{pmatrix} \equiv \bar{e}_{La} \mathcal{M} e_{Ra}, \quad (4)$$

where  $a = 1, \dots, 5$ . Let  $U_L$  and  $U_R$  be unitary matrices that diagonalize the charged lepton mass matrix,

$$U_L^\dagger \mathcal{M} U_R = \begin{pmatrix} M_{e1} & 0 & 0 \\ 0 & M_{e4} & 0 \\ 0 & 0 & M_{e5} \end{pmatrix} \equiv \mathcal{M}^{\text{diag}}. \quad (5)$$

and the mass bases are

$$[\hat{e}_{L,R}]_a = [U_{L,R}^\dagger]_{a,a'} [e_{L,R}]_{a'}. \quad (6)$$

In this model, neutrinos are assumed to only obtain a VL mass term,  $M_L$ .

### Z-lepton Couplings

The  $Z$ -lepton couplings are

$$\mathcal{L} \supset \frac{g}{c_W} Z_\mu [\bar{e}_{La} \gamma^\mu (T_a^3 + s_W^2) e_{La} + \bar{e}_{Ra} \gamma^\mu (T_a^3 + s_W^2) e_{Ra}], \quad (7)$$

where  $s_W = \sin \theta_W$ ,  $c_W = \cos \theta_W$  and  $T_a^3$  is the  $SU(2)$  generator where

$$T_a^3 e_{La} = -\frac{1}{2} \text{diag}(1, 1, 1, 1, 0) e_{La} \equiv T_L^3 e_{La} \quad (8)$$

$$T_a^3 e_{Ra} = -\frac{1}{2} \text{diag}(0, 0, 0, 1, 0) e_{Ra} \equiv T_R^3 e_{Ra}. \quad (9)$$

Since these matrices are not proportional to the identity matrix, when we rotate to the lepton mass basis, the  $Z$ -lepton couplings are not diagonal,

$$\mathcal{L} \supset Z_\mu [\bar{\hat{e}}_{La} \gamma^\mu g_{Lab}^Z \hat{e}_{Lb} + \bar{\hat{e}}_{Ra} \gamma^\mu g_{Rab}^Z \hat{e}_{Rb}] , \quad (10)$$

where  $g_{L,R}^Z = (g/c_W)[U_{L,R}^\dagger(T_{L,R}^3 + s_W^2)U_{L,R}]$ . Hence, this model has LFV  $Z$  boson decays.

### **$W$ -lepton Couplings**

The  $W$ -lepton couplings are

$$\mathcal{L} \supset \frac{g}{\sqrt{2}} W_\mu^+ [\bar{\nu}_{La} \gamma^\mu e_{La} + \bar{\nu}_{Ra} \gamma^\mu e_{Ra}] + \text{h.c.} , \quad (11)$$

where

$$\nu_{La} = \begin{pmatrix} \nu_{Li} \\ L_L^0 \\ 0 \end{pmatrix} , \quad \text{and} \quad \nu_{Ra} = \begin{pmatrix} 0_i \\ L_R^0 \\ 0 \end{pmatrix} . \quad (12)$$

Hence, in the charged lepton mass basis, we have

$$\mathcal{L} \supset W_\mu^+ [\bar{\nu}_{La} \gamma^\mu g_{Lab}^W \hat{e}_{Lb} + \bar{\nu}_{Ra} \gamma^\mu g_{Rab}^W \hat{e}_{Rb}] + \text{h.c.} , \quad (13)$$

where  $g_L^W = (g/\sqrt{2})\text{diag}(1, 1, 1, 1, 0)U_L$  and  $g_R^W = (g/\sqrt{2})\text{diag}(0, 0, 0, 1, 0)U_R$ .

### **Higgs-lepton Couplings**

The couplings between the physical Higgs boson and the leptons are

$$\mathcal{L} \supset -\frac{1}{\sqrt{2}} h \bar{e}_{La} Y_{ab}^e e_{Rb} + \text{h.c.} , \quad (14)$$

where

$$Y^e = \begin{pmatrix} y_{ii}^e & 0 & \lambda_i^E \\ \lambda_i^L & 0 & \lambda \\ 0 & \bar{\lambda} & 0 \end{pmatrix} . \quad (15)$$

In the mass basis, we have

$$\mathcal{L} \supset -\frac{1}{\sqrt{2}} h \bar{\hat{e}}_{La} \hat{Y}_{ab}^e \hat{e}_{Rb} + \text{h.c.} , \quad (16)$$

where

$$\hat{Y}^e = U_L^\dagger Y^e U_R . \quad (17)$$

This Yukawa matrix is non-diagonal because  $Y^e v = \mathcal{M} - \text{diag}(0, 0, 0, M_L, M_E)$ . Hence,

$$\hat{Y}^e = \mathcal{M}^{\text{diag}}/v - U_L^\dagger \text{diag}(0, 0, 0, M_L, M_E) U_R/v , \quad (18)$$

where the second term is non-diagonal.

## Lepton Non-universality

To calculate the effect of this model on lepton non-universality, we consider the following Hamiltonian [7, 8]

$$\mathcal{H}_{\text{eff}} = -\frac{4G_F}{\sqrt{2}} V_{tb} V_{ts}^* \frac{e^2}{16\pi^2} \sum_{j=9,10} C_j \mathcal{O}_j, \quad (19)$$

where

$$\mathcal{O}_9 = (\bar{s}_L \gamma^\mu b_L) (\bar{\hat{e}}_a \gamma_\mu \hat{e}_a), \quad (20)$$

$$\mathcal{O}_{10} = (\bar{s}_L \gamma^\mu b_L) (\bar{\hat{e}}_a \gamma_\mu \gamma_5 \hat{e}_a). \quad (21)$$

The new physics (NP) contribution to these two Wilson coefficients are coming from the box diagrams in Figure 1 (see appendix for calculation [9])

$$\begin{aligned} C_9^{\text{NP}} &= -\frac{1}{s_W^2} \frac{1}{4} [U_1^+(x, y) g_1(x, y) + U_0^+(x, y) g_0(x, y)], \\ C_{10}^{\text{NP}} &= \frac{1}{s_W^2} \frac{1}{4} [U_1^-(x, y) g_1(x, y) + U_0^-(x, y) g_0(x, y)], \end{aligned} \quad (22)$$

where  $x = M_t^2/M_W^2$ ,  $y = M_L^2/M_W^2$ ,

$$Y^{\nu L} \equiv \begin{pmatrix} y_{ii}^e & 0 & \lambda_i^E \\ \lambda_i^L & 0 & \lambda \\ 0 & 0 & 0 \end{pmatrix}, \quad (23)$$

$$Y^{\nu R \dagger} \equiv \begin{pmatrix} 0 & 0 & 0 \\ 0 & 0 & 0 \\ 0 & \bar{\lambda} & 0 \end{pmatrix}, \quad (24)$$

$$g_1(x, y) = \frac{1}{x-y} \left[ \frac{x^2}{(x-1)^2} \log x - \frac{y^2}{(y-1)^2} \log y - \frac{1}{x-1} + \frac{1}{y-1} \right], \quad (25)$$

$$g_0(x, y) = \frac{1}{x-y} \left[ \frac{x}{(x-1)^2} \log x - \frac{y}{(y-1)^2} \log y - \frac{1}{x-1} + \frac{1}{y-1} \right], \quad (26)$$

and

$$U_1^\pm(x, y) = |[U_L]_{4a}|^2 \pm |[U_R]_{4a}|^2 + \frac{1}{4} \frac{v^2}{M_L^2} xy \left( |[Y^{\nu R} U_L]_{4a}|^2 \pm |[Y^{\nu L} U_R]_{4a}|^2 \right), \quad (27)$$

$$\begin{aligned} U_0^\pm(x, y) &= -\frac{v}{M_L} xy \left( [U_L]_{4a} [Y^{\nu R*} U_L^*]_{4a} + [U_L^*]_{4a} [Y^{\nu R} U_L]_{4a} \right. \\ &\quad \left. \pm [U_R]_{4a} [Y^{\nu L*} U_R^*]_{4a} \pm [U_R^*]_{4a} [Y^{\nu L} U_R]_{4a} \right). \end{aligned} \quad (28)$$

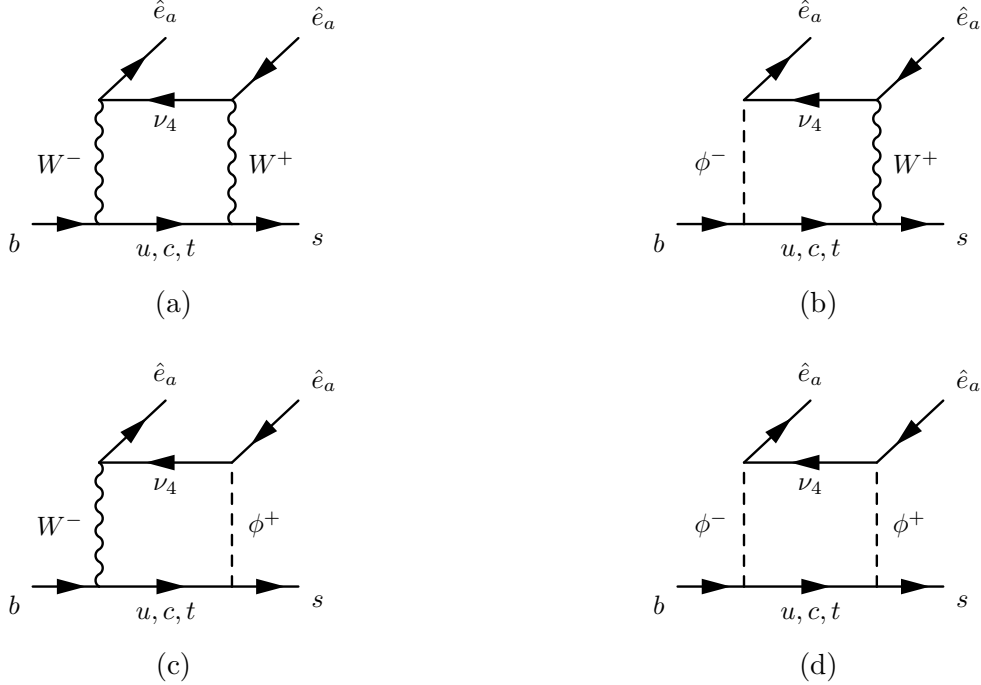


Figure 1: Box diagrams contributing to  $b \rightarrow s \hat{e}_a \hat{e}_a$ .

### 3 PROCEDURE

The analysis of this paper is similar to that in [2]. A new feature of this paper is that VL leptons are not assumed to couple exclusively to muons. Instead, VL leptons couple to all three families of SM leptons and we are interested in the constraints of the 10 model parameters: VL Masses,  $M_{L,E}$ ; VL-VL couplings,  $\lambda, \bar{\lambda}$ ; and SM-VL couplings,  $\lambda_{e,\mu,\tau}^{L,E}$ .  $y_{e,\mu,\tau}$  are not free parameters because  $y_{e,\mu,\tau}$  are chosen such that  $m_{e,\mu,\tau}$  are the central values in Particle Data Group (PDG) [1]. We considered  $M_{L,E} \in (100, 1000)$  GeV and  $\lambda, \bar{\lambda} \in (-1, 1)$ . As for the SM-VL couplings, we considered

$$\frac{\lambda_{e,\mu,\tau}^{L,E} v}{M_{L,E}} \in (-0.09, 0.09). \quad (29)$$

The ranges of the SM-VL couplings are chosen to satisfy the electroweak constraints.<sup>1</sup>

The constraints that we consider in this paper are from the heavy charged lepton mass bound, precision electroweak data, the muon  $g - 2$ , LFV, Higgs decays, and lepton non-universality observables. See Table 2 for the complete list of observables. All of the experimental values, other than lepton non-universality observables, are taken from the PDG [1].

<sup>1</sup>With our upper limit on  $M_{L,E} = 1000$  GeV, this implies an upper bound on the dimensionless couplings  $\lambda_{e,\mu,\tau}^{L,E} \lesssim 0.5$ .

The experimental value for  $R_K$  is taken from Reference [10], while  $R_{K^*0}$  is recently measured by LHCb [11].

The heavy charged lepton mass bound quoted by the PDG,  $M > 100.8 \text{ GeV}$ , is from the LEP experiment. There are more recent bounds on the mass of VL leptons obtained from reinterpreting ATLAS and CMS experiments [12–15]. If the lightest VL lepton is predominantly  $E_{L,R}$ , then the bound is similar to the LEP bound. However, if the lightest VL lepton is predominantly  $L_{L,R}$ , then the bound can be more stringent. For example, Falkowski et. al. showed that if the VL lepton decays only to  $e$  and  $\mu$ , then the bound is  $M_{e4} \gtrsim 450 \text{ GeV}$  [12]. On the other hand, Kumar et. al. showed that if the VL lepton decays only to  $\tau$ , then the bound may only be  $M_{e4} \gtrsim 275 \text{ GeV}$  [15]. Due to the sampling method that we explain below, VL leptons in this model can either be predominantly  $E_{L,R}$  or  $L_{L,R}$ , depending on model parameters. In addition, VL leptons of this model can decay to all three SM leptons. Hence, reinterpretations of the ATLAS and CMS analyses are needed to obtain the bound on this model. To be conservative, we have decided to use the LEP bound in this paper while keeping in mind that more stringent bounds may exist.

All theoretical calculations are performed at leading order, that is all observables other than  $\Delta a_\mu, \text{BR}(\ell \rightarrow \ell' \gamma), R_{\gamma\gamma}, R_K, R_{K^*0}$  are calculated at tree level. The effect of one-loop calculations are expected to be small. The theoretical calculation of the VL contribution to the muon  $g - 2$  is taken from Reference [2]. The calculation for  $\text{BR}(\ell \rightarrow \ell' \gamma)$  and  $R_{\gamma\gamma}$  are performed at one-loop [16, 17]. Since all calculations are performed at leading order, we have included a 1% theoretical error when ensuring that the calculated observables satisfy the current experimental bounds. As for the lepton non-universality analysis, we have used `flavio`, a very versatile program that calculates  $b$ -physics observables written by Straub et. al. [18]. To calculate the NP effects of the observables implemented in `flavio`, one only has to specify the NP contribution to the Wilson coefficients.

In the analysis, we obtain scatter plots by sampling from the parameter space and checking to see if the sampled points satisfy the constraints mentioned above. To ensure that we cover all regions in this vast parameter space, we divide VL masses into four different regions:  $M_{L,E} \in [100, 150), [150, 250), [250, 500), [500, 1000) \text{ GeV}$ , and the VL-VL couplings into two different regions<sup>2</sup>:  $|\lambda|, |\bar{\lambda}| \in [0, 0.75), [0.75, 1)$ . As for the muon-VL couplings, we considered  $|\lambda_\mu^{L,E} v / M_{L,E}| \in [0, 0.06), [0.06, 0.09)$ . For each of these regions, we sampled 10,000 points satisfying the heavy charged lepton mass bound and the electroweak precision observables. The total number of simulated points is 2.56 millions points. The parameters  $M_{L,E}, \lambda, \bar{\lambda}, \lambda_\mu^{L,E}$  are sampled from a uniform distribution while  $|\lambda_{e,\tau}^{L,E} v / M_{L,E}| \in [10^{-10}, 0.09)$  are sampled from a log-uniform distribution. The electron-VL and tau-VL couplings are

---

<sup>2</sup>These couplings can be positive or negative. The quoted ranges are the magnitude. Similarly for SM-VL couplings.

sampled from a log-uniform distribution because we expect these couplings to be highly constrained by LFV observables and we are interested in determining the degree of fine-tuning of these two parameters in order to be consistent with the flavor violation constraints.

Muon $g - 2$	$\mu$	$\Delta a_\mu$
Heavy Charged Leptons	$e_4$	$M_{e4}$
Electroweak Precision	$Z$	$A_{e,\mu,\tau}, A_{FB}^{(0e),(0\mu),(0\tau)}$ $\text{BR}(Z \rightarrow ee), \text{BR}(Z \rightarrow \mu\mu), \text{BR}(Z \rightarrow \tau\tau)$
	$W$	$\text{BR}(W \rightarrow e\nu_e), \text{BR}(W \rightarrow \mu\nu_\mu), \text{BR}(W \rightarrow \tau\nu_\tau)$
	$\mu$	$\text{BR}(\mu \rightarrow e\bar{\nu}_e\nu_\mu)$
	$\tau$	$\text{BR}(\tau \rightarrow e\bar{\nu}_e\nu_\tau), \text{BR}(\tau \rightarrow \mu\bar{\nu}_\mu\nu_\tau)$
Lepton Flavor Violation	$Z$	$\text{BR}(Z \rightarrow e\mu), \text{BR}(Z \rightarrow e\tau), \text{BR}(Z \rightarrow \mu\tau)$
	$\mu$	$\text{BR}(\mu \rightarrow e\gamma), \text{BR}(\mu \rightarrow 3e)$
	$\tau$	$\text{BR}(\tau \rightarrow e\gamma), \text{BR}(\tau \rightarrow \mu\gamma)$ $\text{BR}(\tau \rightarrow 3e), \text{BR}(\tau \rightarrow 3\mu)$
Higgs	$h$	$R_{\mu\mu}, R_{\tau\tau}, R_{\gamma\gamma}, \text{BR}(h \rightarrow \mu\tau)$
Lepton Non-Universality	$B$ meson	$R_K, R_{K^*0}$

Table 2: List of observables.  $\Delta a_\mu$  is the discrepancy of the measured muon  $g - 2$  and the SM prediction.  $A_{e,\mu,\tau}$  is the electron, muon, and tau left-right asymmetry in  $Z$  decay.  $A_{FB}^{(0e),(0\mu),(0\tau)}$  is the electron, muon, and tau forward-backward asymmetry in  $Z$  decay.  $R_{\mu\mu} = \Gamma(h \rightarrow \mu\mu)/\Gamma(h \rightarrow \mu\mu)_{\text{SM}}$  and similarly for  $R_{\tau\tau}$  and  $R_{\gamma\gamma}$ .  $R_K = \Gamma(B^+ \rightarrow K^+\mu\mu)/\Gamma(B^+ \rightarrow K^+ee)$  while  $R_{K^*0} = \Gamma(B^0 \rightarrow K^{*0}\mu\mu)/\Gamma(B^0 \rightarrow K^{*0}ee)$ . Lepton non-universality experimental values are taken from LHCb measurements [10, 11] while the other experimental values are taken from PDG [1].

## 4 RESULTS

In this section, we present the results of our numerical analysis. For all plots in this section, we have classified the simulated points into two groups. This classification is based on whether a point satisfies all observables listed in Table 2 other than the plotted observables and the lepton non-universality observables. The lightly shaded points do not satisfy one or more of these observables while the solid colored points satisfy all these observables.

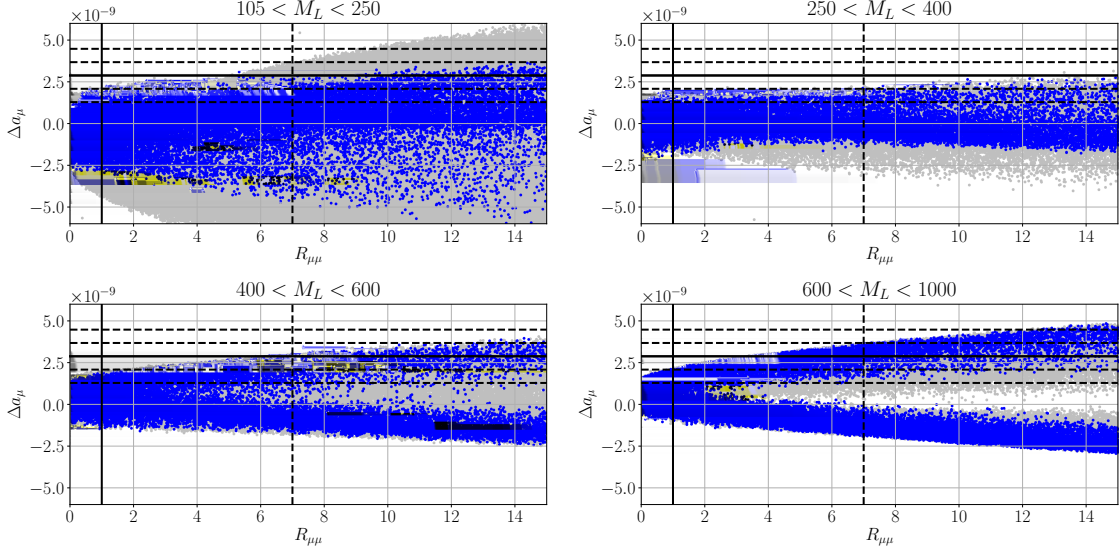


Figure 2: Plots of the muon  $g-2$  discrepancy,  $\Delta a_\mu$ , versus  $R_{\mu\mu} = \Gamma(h \rightarrow \mu\mu)/\Gamma(h \rightarrow \mu\mu)_{\text{SM}}$ . The four plots have different ranges of  $M_L$ . The gray points are ruled out. The dashed lines show the  $1\sigma$  and  $2\sigma$  bounds of  $\Delta a_\mu$  and the upper bound of  $R_{\mu\mu}$ . The solid lines show the central value of  $\Delta a_\mu$  and  $R_{\mu\mu} = 1$ .

Figure 2 shows plots of  $\Delta a_\mu$  versus  $R_{\mu\mu}$ . The four plots have different ranges of  $M_L$ , which is a meaningful discriminator because the VL contribution to the muon  $g-2$  from the  $W$  boson loop is due to the  $SU(2)$  doublet VL neutrinos,  $L_{L,R}^0$ , which have mass  $M_L$  [2]. The dashed lines show the  $1\sigma$  and  $2\sigma$  bounds of  $\Delta a_\mu$ , and the upper bound of  $R_{\mu\mu}$ . The solid lines show the central value of  $\Delta a_\mu$  and  $R_{\mu\mu} = 1$ .<sup>3</sup> From this figure, we see that this model can be ruled out in the future if future measurements of the muon  $g-2$  and  $R_{\mu\mu}$  have much smaller uncertainties, and  $R_{\mu\mu}$  is measured to be SM-like while the muon  $g-2$  is measured to have a similar central value.

Figure 2 also shows that there are no points with  $250 \text{ GeV} < M_L < 400 \text{ GeV}$  that fit the muon  $g-2$  within  $1\sigma$ .<sup>4</sup> This observation is further illustrated in Figure 3, which shows plots of  $\Delta a_\mu$  versus  $M_L$ . The two plots have different ranges of  $\bar{\lambda}$ . This figure shows that for  $\bar{\lambda} < 0.25$ , this model requires either  $M_L < 250 \text{ GeV}$  or  $M_L > 600 \text{ GeV}$  to fit the muon  $g-2$  within  $1\sigma$ . On the other hand, this model requires  $M_L > 400 \text{ GeV}$  for  $\bar{\lambda} > 0.25$ . This plot also shows that the allowed parameter space for  $M_L \lesssim 250 \text{ GeV}$  can potentially be eliminated by the upcoming Fermilab E989 experiment if the muon  $g-2$  central value stays

<sup>3</sup>Notice that there is no measurement of  $R_{\mu\mu}$  yet. There is only an upper bound.

<sup>4</sup>The bounds on parameter space obtained are not strict because the analysis is performed by random sampling from the vast parameter space. Our sampling method attempts to cover the whole parameter space but there might still be regions which are missed by the sampling method.

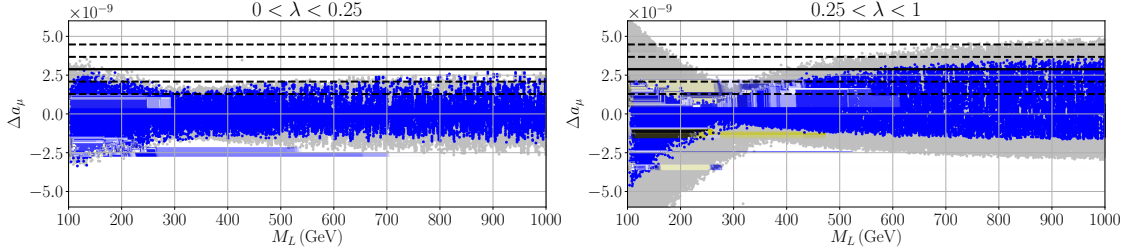


Figure 3: Plots of  $\Delta a_\mu$  versus  $M_L$ . The two plots have different ranges of  $\bar{\lambda}$ . The gray points are ruled out. The dashed lines are the  $1\sigma$  and  $2\sigma$  bounds of  $\Delta a_\mu$  while the solid line is the central value of  $\Delta a_\mu$ .

the same while the uncertainties decrease by a couple factors [19].

In general, as the VL masses increase, the new physics effects should approach zero. However, Figure 3 seems to violate this fact. The muon  $g - 2$  does not approach zero as  $M_L$  increases because other parameters, such as  $M_E$ ,  $\bar{\lambda}$ , and  $\lambda_\mu^{L,E}$ , are not fixed. In fact, if all the other parameters are fixed, then the muon  $g - 2$  approaches zero as  $M_L$  increases.

Figure 4 shows a plot of  $\Delta a_\mu$  versus  $R_{\gamma\gamma}$ . The points in this plot are separated into different colors based on  $M_{e4}$ . As expected, for heavier VL mass eigenstates,  $R_{\gamma\gamma}$  is clustered around one. This plot shows that  $M_{e4} > 500$  GeV is a more robust region than regions with smaller  $M_{e4}$  because a larger percentage of simulated points are within the experimental bounds. A very interesting scenario will arise if the central value of  $R_{\gamma\gamma}$  stays and uncertainties in the measurement decrease as more data are collected. In this scenario, we will have the potential to place an upper bound on the mass of the lightest VL mass eigenstate because there are no points with  $M_{e4} > 500$  GeV and  $R_{\gamma\gamma} \gtrsim 1.1$ .

In Figure 5, which shows plots of  $\Delta a_\mu$  versus  $R_{\gamma\gamma}$ , the points are separated into four different plots based on different values of

$$\|\lambda_\mu\| \equiv \sqrt{\left(\frac{\lambda_\mu^L v}{M_L}\right)^2 + \left(\frac{\lambda_\mu^E v}{M_E}\right)^2}. \quad (30)$$

$\|\lambda_\mu\|$  is a meaningful variable because muon-VL couplings plays a significant role in fitting  $\Delta a_\mu$  and this variable captures the norm of the muon-VL coupling normalized by the VL masses. From this figure, we see that this model requires  $\|\lambda_\mu\| > 0.03$  to fit  $\Delta a_\mu$  within  $1\sigma$  and  $\|\lambda_\mu\| < 0.09$  to fit  $R_{\gamma\gamma}$ .

Figure 6 shows a plot of  $\lambda_\mu^L$  versus  $\lambda_\mu^E$ . The gray points are all simulated points. The red points satisfy  $\Delta a_\mu$  within  $1\sigma$  while the blue points are consistent with  $\Delta a_\mu$  and  $R_{\gamma\gamma}$ .<sup>5</sup> To

<sup>5</sup>The square shape in Figure 6 is unphysical and is due to our choice of sampling range.

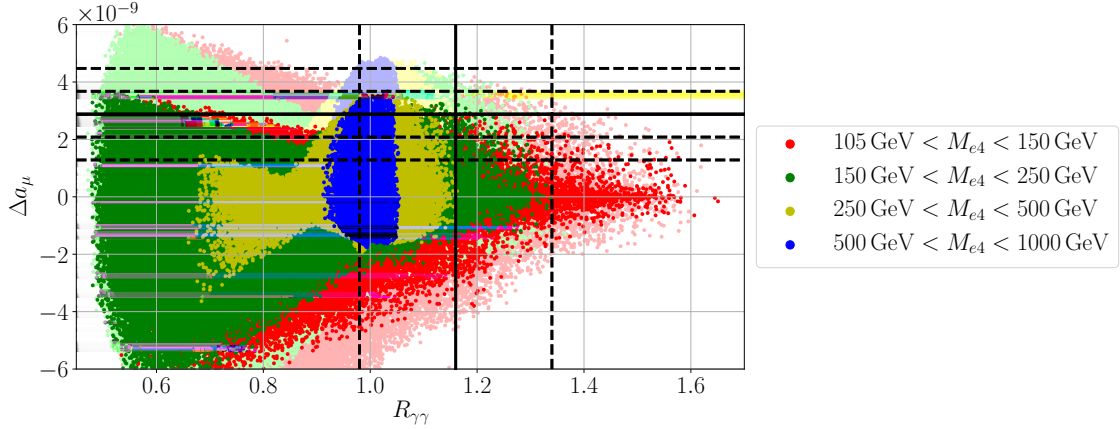


Figure 4: Plot of  $\Delta a_\mu$  versus  $R_{\gamma\gamma}$ . The lightly shaded points are ruled out. The dashed lines show the  $1\sigma$  and  $2\sigma$  bounds of  $\Delta a_\mu$ , and the  $1\sigma$  bound of  $R_{\gamma\gamma}$ . The solid lines show the central value of  $\Delta a_\mu$  and that of  $R_{\gamma\gamma}$ .

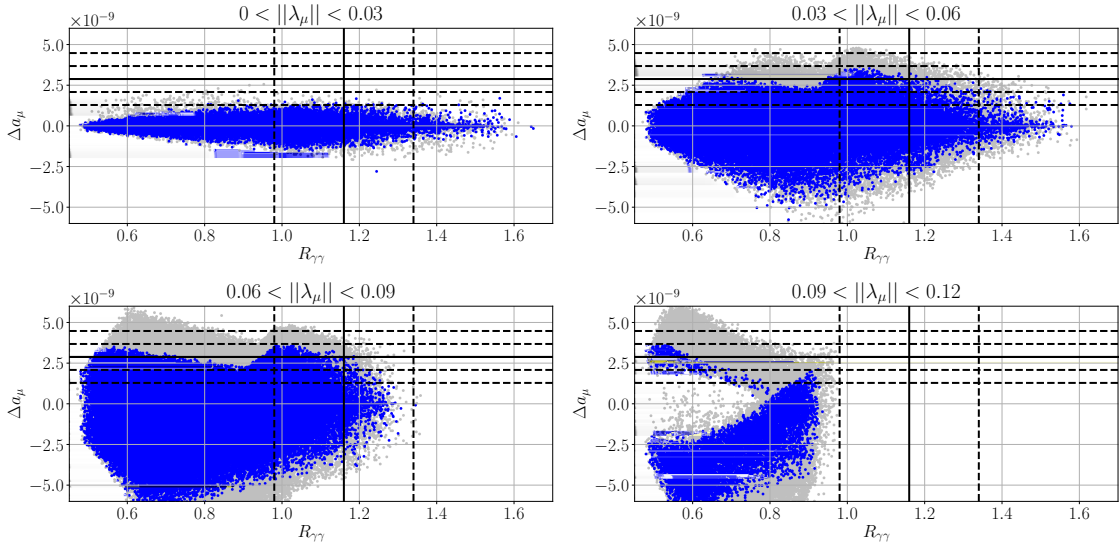


Figure 5: Plots of  $\Delta a_\mu$  versus  $R_{\gamma\gamma}$ . The gray points are ruled out. The dashed lines show the  $1\sigma$  and  $2\sigma$  bounds of  $\Delta a_\mu$ , and the  $1\sigma$  bound of  $R_{\gamma\gamma}$ . The solid lines show the central value of  $\Delta a_\mu$  and that of  $R_{\gamma\gamma}$ . This model requires  $||\lambda_\mu|| > 0.03$  to fit  $\Delta_\mu$  and  $||\lambda_\mu|| < 0.09$  to fit  $R_{\gamma\gamma}$ .

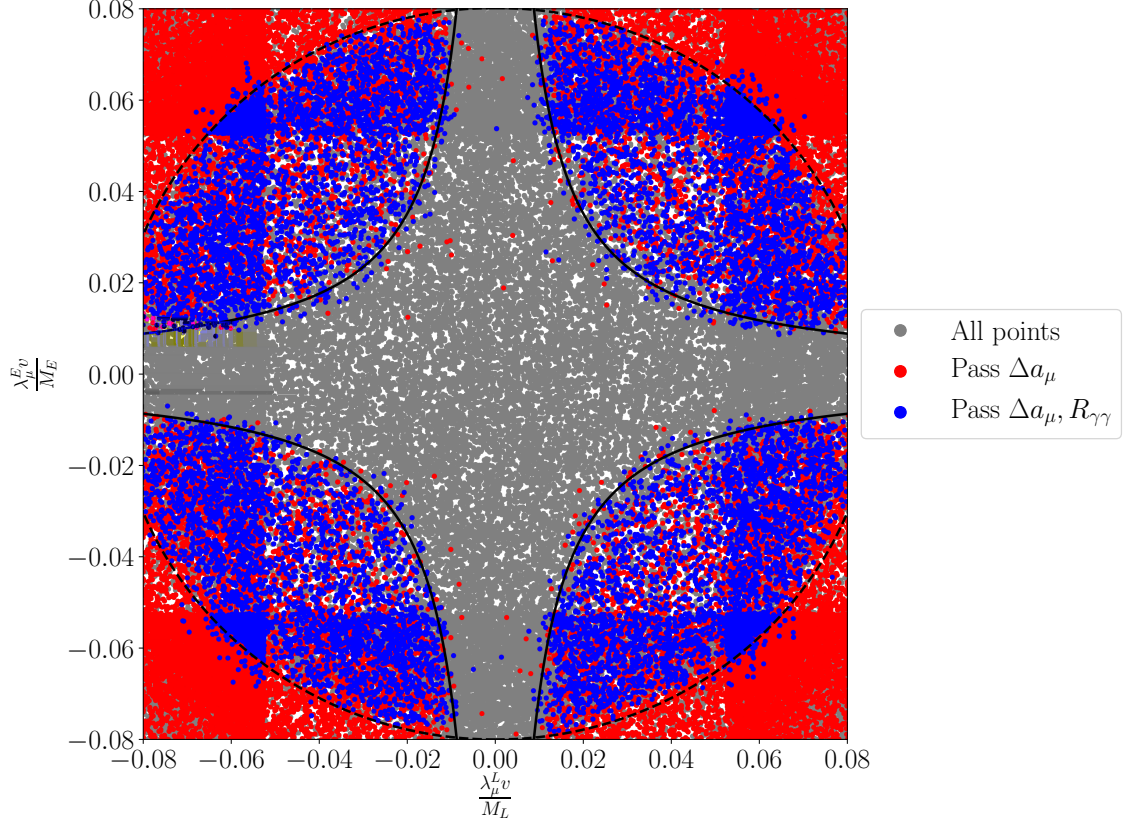


Figure 6: Plot of the muon- $\nu L$  couplings,  $\lambda_\mu^E v / M_E$  versus  $\lambda_\mu^L v / M_L$ . The solid and dashed black lines are the approximate empirical bounds on the muon- $\nu L$  couplings. These bounds are not exact, but are obtained empirically (see text for more discussions).

satisfy  $\Delta a_\mu$ , the muon- $\nu L$  couplings need to satisfy approximately the following condition,

$$\left| \frac{\lambda_\mu^E v}{M_E} \frac{\lambda_\mu^L v}{M_L} \right| \gtrsim 7 \times 10^{-4}, \quad (31)$$

which is shown by the solid lines. This bound is not an exact bound, but is an empirically obtained bound satisfied by most simulated points. On the other hand, to satisfy both  $\Delta a_\mu$  and  $R_{\gamma\gamma}$ , the muon- $\nu L$  couplings need to satisfy approximately the following condition,

$$\left( \frac{\lambda_\mu^E v}{M_E} \right)^2 + \frac{1}{1.08} \left( \frac{\lambda_\mu^L v}{M_L} \right)^2 \lesssim 0.08^2, \quad (32)$$

which is showed by the dashed black lines. Similarly, this is not an exact bound.

Figure 7 shows a plot of  $\Delta a_\mu$  versus  $\text{BR}(\mu \rightarrow e\gamma)$ , which gives the strongest LFV constraint. The points in this plot are separated into four colors based on ranges of the ratio of

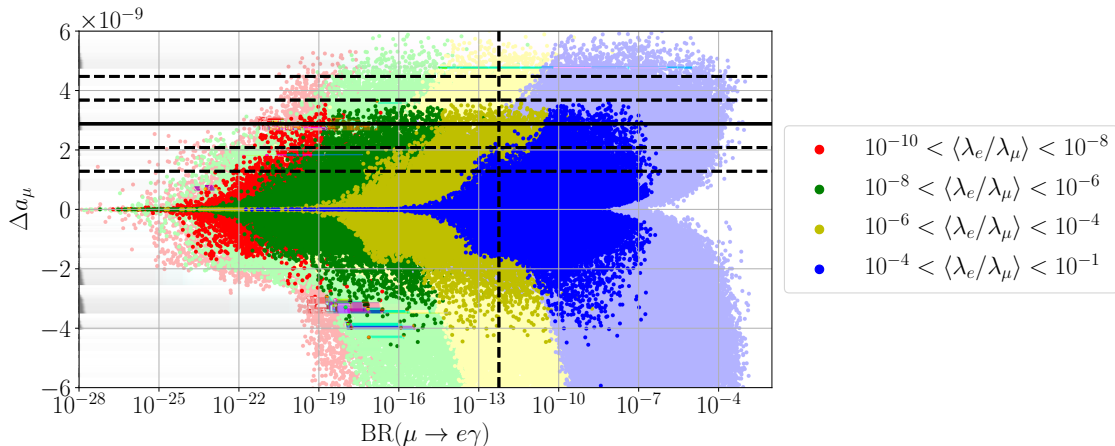


Figure 7: Plot of  $\Delta a_\mu$  versus  $\text{BR}(\mu \rightarrow e\gamma)$ , which gives the strongest LFV constraint. The lightly shaded points are ruled out. The dashed lines show the  $1\sigma$  and  $2\sigma$  bounds of  $\Delta a_\mu$ , and the upper bound of  $\text{BR}(\mu \rightarrow e\gamma)$ . The solid line shows the central value of  $\Delta a_\mu$ . Simultaneously satisfying  $\text{BR}(\mu \rightarrow e\gamma)$  and  $\Delta a_\mu$  to within  $1\sigma$  require  $\langle \lambda_e/\lambda_\mu \rangle \lesssim 10^{-4}$ .

electron-VL to muon-VL couplings,

$$\left\langle \frac{\lambda_e}{\lambda_\mu} \right\rangle \equiv \frac{1}{2} \left( \frac{\lambda_e^L}{\lambda_\mu^L} + \frac{\lambda_e^E}{\lambda_\mu^E} \right). \quad (33)$$

The dashed lines show the  $1\sigma$  and  $2\sigma$  bounds of  $\Delta a_\mu$ , and the upper bound of  $\text{BR}(\mu \rightarrow e\gamma)$ . The solid line shows the central value of  $\Delta a_\mu$ . This figure shows that simultaneously satisfying  $\text{BR}(\mu \rightarrow e\gamma)$  and  $\Delta a_\mu$  to within  $1\sigma$  require  $\langle \lambda_e/\lambda_\mu \rangle \lesssim 10^{-4}$ .<sup>6</sup> This figure shows that this model requires some level of fine-tuning.

The most stringent constraints for the tau-VL coupling is from electroweak observables. The sampling range for tau-VL couplings,  $\lambda_\tau^{L,E} v/M_{L,E} \in (-0.09, 0.09)$ , is based on electroweak constraints. The next strongest constraint for the tau-VL coupling is  $\text{BR}(\tau \rightarrow \mu\gamma)$ . This constraint, however, does not rule out any value of the tau-VL couplings within the sampling range. Finally,  $\text{BR}(h \rightarrow \mu\tau)$  does not constrain the parameter space at all. This is in agreement with a previous analysis by Falkowski et. al., which shows that the constraint from LFV Higgs decays is at least four orders of magnitude smaller than that from  $\text{BR}(\ell \rightarrow \ell'\gamma)$  [12].

As for the lepton non-universality measurements, the calculated values of  $R_K$  and  $R_{K^*0}$  do not deviate from the SM predictions because the Wilson coefficients contain the SM-VL mixing matrices squared, which are highly constrained by electroweak precision measure-

<sup>6</sup>Out of all simulated points, four points that violate this bound with the largest violation being  $\langle \lambda_e/\lambda_\mu \rangle = 2 \times 10^{-4}$ .

ments. The ranges of Wilson coefficients in this model are

$$\begin{aligned}
-3.21 \times 10^{-11} &\leq C_9^{\text{NP}}(e) \leq 7.26 \times 10^{-12}, \\
-3.21 \times 10^{-11} &\leq C_{10}^{\text{NP}}(e) \leq 7.26 \times 10^{-12}, \\
-7.88 \times 10^{-3} &\leq C_9^{\text{NP}}(\mu) \leq 2.21 \times 10^{-3}, \\
-7.86 \times 10^{-3} &\leq C_{10}^{\text{NP}}(\mu) \leq 2.18 \times 10^{-3}.
\end{aligned}
\tag{34}$$

As a comparison, to fit all the CP-conserving  $b \rightarrow s\mu^+\mu^-$  anomalies along with  $R_K$  and  $R_{K^*0}$ , the Wilson coefficients need to have values  $C_9^{\text{NP}}(\mu) = -1.20 \pm 0.20$  and  $C_9^{\text{NP}}(e) = C_{10}^{\text{NP}}(e) = C_{10}^{\text{NP}}(\mu) = 0$ , or  $C_9^{\text{NP}}(\mu) = -C_{10}^{\text{NP}}(\mu) = -0.68 \pm 0.12$  and  $C_9^{\text{NP}}(e) = C_{10}^{\text{NP}}(e) = 0$  [20].

## 5 CONCLUSION

In this paper, we considered a very simple extension of the SM in which the SM is extended with one family of VL leptons; where the VL leptons couple to all three families of SM leptons. We studied the constraints on this model coming from the heavy charged lepton mass bound, electroweak precision data, the muon  $g - 2$ , lepton flavor violation, Higgs decays and lepton non-universality observables. See Table 2 for the complete list of observables considered in this paper. All experimental values, other than lepton non-universality observables, are taken from the PDG [1]. The experimental value for  $R_K$  is taken from Reference [10], while  $R_{K^*0}$  is recently measured by LHCb [11]. All theoretical calculations are performed at leading order while the lepton non-universality observables are calculated using `flavio` [18].

In this paper, we showed that this model can fit all but the lepton non-universality measurements. The most constraining observables are the muon  $g - 2$ ,  $R_{\mu\mu}$ ,  $R_{\gamma\gamma}$  and the  $\text{BR}(\mu \rightarrow e\gamma)$ . We find that if  $R_{\mu\mu}$  is measured to be SM-like, then this model cannot simultaneously fit both the muon  $g - 2$  within  $1\sigma$  and  $R_{\mu\mu}$  (see Figure 2). In addition, we also find that the SU(2) doublet VL mass is required to satisfy  $M_L \lesssim 250 \text{ GeV}$  or  $M_L \gtrsim 400 \text{ GeV}$  in order to fit the muon  $g - 2$  within  $1\sigma$  (see Figure 3). If the heavy charged lepton mass bound increases to be above  $M_L \gtrsim 250 \text{ GeV}$ , then the muon  $g - 2$  can produce a stronger mass bound. Fitting to the muon  $g - 2$  requires  $|\lambda_\mu| > 0.03$  while fitting to  $R_{\gamma\gamma}$  requires  $|\lambda_\mu| < 0.09$ . Hence, the muon-VL coupling is constrained to be within  $0.03 < |\lambda_\mu| < 0.09$ . Although we allow the VL leptons to couple to all three families of the SM leptons, by simultaneously fitting the muon  $g - 2$  and  $\text{BR}(\mu \rightarrow e\gamma)$ , the ratio of the electron-VL coupling to muon-VL coupling is constrained to be  $\langle \lambda_e/\lambda_\mu \rangle \lesssim 10^{-4}$ . Hence, this model requires some level of fine-tuning. On the other hand, the strongest constraints on the tau-VL coupling is coming from electroweak precision observables. The recently measured  $\text{BR}(h \rightarrow \mu\tau)$  is less constraining than the electroweak precision observables. We also find that this model cannot explain the B physics lepton non-universality measurements.

## ACKNOWLEDGMENTS

Z.P. and S.R. received partial support for this work from DOE/DE-SC0011726. We would like to thank Andrzej Buras and Hong Zhang for discussions.

# A BOX DIAGRAM CALCULATION

In this appendix, we calculate four box diagrams that have NP contributions to the decay of  $b \rightarrow s\ell\ell$ . As shown in Figure 1, the NP contributions of these diagrams are due to VL leptons in the loop. The NP contribution enters via Wilson coefficients  $C_9$  and  $C_{10}$ . The calculation in this appendix is done in the 't Hooft-Feynman gauge.

## A.1 Feynman Rules

To see all the Feynman rules explicitly, we start by rewriting the Lagrangian that is relevant to our calculation. The definition of the fields and their corresponding quantum numbers are given in Table 1. The Lagrangian of the leptonic sector is given in Eq. 3.

### W-lepton Couplings

From Eq. 13, we have

$$\mathcal{L} \supset \frac{g}{\sqrt{2}} \left[ W_\mu^+ \bar{\nu}_a \gamma^\mu ([\tilde{U}_L]_{ab} P_L + [\tilde{U}_R]_{ab} P_R) \hat{e}_b + W_\mu^- \bar{\hat{e}}_b \gamma^\mu ([\tilde{U}_L^*]_{ab} P_L + [\tilde{U}_R^*]_{ab} P_R) \nu_a \right], \quad (35)$$

where  $P_{L,R}$  are projection operators and

$$\tilde{U}_L = \text{diag}(1, 1, 1, 1, 0) U_L \quad (36)$$

$$\tilde{U}_R = \text{diag}(0, 0, 0, 1, 0) U_R. \quad (37)$$

Notice that  $[U_L]_{4a} = [\tilde{U}_L]_{4a}$ , where  $a = 1, \dots, 5$ . Similarly for  $U_R$ .

### Higgs-lepton Couplings

Rewriting the Lagrangian, Eq. 3, in terms of the physical Higgs and the would-be Nambu-Goldstone bosons gives

$$\begin{aligned} \mathcal{L} \supset & - \left( v + \frac{h}{\sqrt{2}} \right) \bar{e}_{L_a} Y_{ab}^e e_{R_b} - \frac{i\phi^0}{\sqrt{2}} \bar{e}_{L_a} Y_{ab}^{e\phi^0} e_{R_b} \\ & - \phi^+ \bar{\nu}_{L_b} Y_{ba}^{\nu L} e_{R_a} - \phi^- \bar{e}_{L_a} Y_{ab}^{\nu R \dagger} \nu_{R_b} + \text{h.c.} . \end{aligned} \quad (38)$$

where  $Y^e$ ,  $Y^{\nu L}$ , and  $Y^{\nu R \dagger}$  are given by Eq. 15, Eq. 23, and Eq. 24 respectively, and

$$Y^{e\phi^0} \equiv \begin{pmatrix} y_{ii}^e & 0 & \lambda_i^E \\ \lambda_i^L & 0 & \lambda \\ 0 & -\bar{\lambda} & 0 \end{pmatrix}. \quad (39)$$

In the charged lepton mass basis, we have

$$\begin{aligned} \mathcal{L} \supset & - \left( v + \frac{h}{\sqrt{2}} \right) \bar{\tilde{e}}_{L_a} \hat{Y}_{ab}^e \hat{e}_{R_b} - \frac{i\phi^0}{\sqrt{2}} \bar{\tilde{e}}_{L_a} [U_L^\dagger Y^{e\phi^0} U_R]_{ab} \hat{e}_{R_b} \\ & - \phi^+ \bar{\nu}_{L_b} [Y^{\nu L} U_R]_{ba} \hat{e}_{R_a} - \phi^- \bar{\tilde{e}}_{L_a} [U_L^\dagger Y^{\nu R^\dagger}]_{ab} \nu_{R_b} + \text{h.c.} . \end{aligned} \quad (40)$$

So, the Feynman rules for the coupling in diagrams (b)-(d) in Figure 1 involving the charged would-be Nambu-Goldstone bosons are

$$\phi^+ : -i([Y^{\nu L} U_R]_{4a} P_R + [Y^{\nu R} U_L]_{4a} P_L) , \quad (41)$$

$$\phi^- : -i([Y^{\nu L*} U_R^*]_{4a} P_L + [Y^{\nu R*} U_L^*]_{4a} P_R) . \quad (42)$$

Since all the calculations are performed in the charged lepton mass basis, to simplify notation, we will drop  $\hat{\phantom{x}}$  in the rest of this appendix.

## A.2 Loop Calculations

Before we start to evaluate the four diagrams in Figure 1, let's consider two loop integrals that we will be using. These loop integrals are performed easily with `Package-X` developed by Patel [21].

$$A_{\alpha\beta}(M_i, M_L) \equiv \int \frac{d^4 q}{(2\pi)^4} \frac{q_\alpha q_\beta}{(q^2 - M_W^2)^2 (q^2 - M_i^2) (q^2 - M_L^2)} = -\frac{i}{64\pi^2 M_W^2} g_1(x_i, y) g_{\alpha\beta} , \quad (43)$$

$$B(M_i, M_L) \equiv \int \frac{d^4 q}{(2\pi)^4} \frac{1}{(q^2 - M_W^2)^2 (q^2 - M_i^2) (q^2 - M_L^2)} = -\frac{i}{16\pi^2 M_W^4} g_0(x_i, y) , \quad (44)$$

where  $x_i = M_i^2/M_W^2$ ,  $y = M_L^2/M_W^2$  and

$$g_1(x, y) = \frac{1}{x-y} \left[ \frac{x^2}{(x-1)^2} \log x - \frac{y^2}{(y-1)^2} \log y - \frac{1}{x-1} + \frac{1}{y-1} \right] , \quad (45)$$

$$g_0(x, y) = \frac{1}{x-y} \left[ \frac{x}{(x-1)^2} \log x - \frac{y}{(y-1)^2} \log y - \frac{1}{x-1} + \frac{1}{y-1} \right] . \quad (46)$$

### Diagram (a)

$$\begin{aligned} \square^{(a)} &= \left( \frac{g}{\sqrt{2}} \right)^4 \sum_{i=u,c,t} V_{ib} V_{is}^* \int \frac{d^4 q}{(2\pi)^4} \left( \frac{-i}{q^2 - M_W^2} \right)^2 \left[ \bar{s} \gamma^\mu P_L \frac{i(\not{q} + M_i)}{q^2 - M_i^2} \gamma^\nu P_L b \right] \\ &\quad \left[ \bar{e}_a ([U_L^*]_{4a} \gamma_\nu P_L + [U_R^*]_{4a} \gamma_\nu P_R) \frac{i(\not{q} + M_L)}{q^2 - M_L^2} ([U_L]_{4a} \gamma_\mu P_L + [U_R]_{4a} \gamma_\mu P_R) e_a \right] \\ &= \frac{g^4}{4} \sum_{i=u,c,t} V_{ib} V_{is}^* \int \frac{d^4 q}{(2\pi)^4} \frac{1}{(q^2 - M_W^2)^2 (q^2 - M_i^2) (q^2 - M_L^2)} \\ &\quad [\bar{s} \gamma^\mu P_L (\not{q} + M_i) \gamma^\nu P_L b] \\ &\quad [\bar{e}_a ([U_L^*]_{4a} \gamma_\nu P_L + [U_R^*]_{4a} \gamma_\nu P_R) (\not{q} + M_L) ([U_L]_{4a} \gamma_\mu P_L + [U_R]_{4a} \gamma_\mu P_R) e_a] . \end{aligned}$$

The last two square brackets can be written as

$$q_\alpha q_\beta [\bar{s}\gamma^\mu \gamma^\alpha \gamma^\nu P_L b] [\bar{e}_a \gamma_\nu \gamma^\beta \gamma_\mu (|[U_L]_{4a}|^2 P_L + |[U_R]_{4a}|^2 P_R) e_a],$$

where we have dropped terms linear in  $q$ . Using Eq. 43,

$$\begin{aligned} \square^{(a)} &= \frac{g^4}{4} \sum_{i=u,c,t} V_{ib} V_{is}^* A_{\alpha\beta}(M_i, M_L) [\bar{s}\gamma^\mu \gamma^\alpha \gamma^\nu P_L b] \\ &\quad [\bar{e}_a \gamma_\nu \gamma^\beta \gamma_\mu (|[U_L]_{4a}|^2 P_L + |[U_R]_{4a}|^2 P_R) e_a]. \end{aligned}$$

Using  $g_{\alpha\beta}$  from  $A_{\alpha\beta}$ , the last two square brackets can be written as

$$[\bar{s}\gamma^\mu \gamma^\alpha \gamma^\nu P_L b] [\bar{e}_a \gamma_\nu \gamma_\alpha \gamma_\mu (|[U_L]_{4a}|^2 P_L + |[U_R]_{4a}|^2 P_R) e_a].$$

Using the following Dirac matrix identity,

$$\gamma^\mu \gamma^\alpha \gamma^\nu = g^{\mu\alpha} \gamma^\nu + g^{\alpha\nu} \gamma^\mu - g^{\mu\nu} \gamma^\alpha - i\epsilon^{\beta\mu\alpha\nu} \gamma_\beta \gamma^5,$$

we can rewrite the last two square brackets as

$$4[\bar{s}\gamma^\mu P_L b] [\bar{e}_a \gamma_\mu (|[U_L]_{4a}|^2 P_L + |[U_R]_{4a}|^2 P_R) e_a].$$

Putting all these together, we have

$$\begin{aligned} \square^{(a)} &= -i \frac{4G_F}{\sqrt{2}} \sum_{i=u,c,t} V_{ib} V_{is}^* \frac{e^2}{16\pi^2} \frac{1}{s_W^2} \frac{1}{2} g_1(x_i, y) \\ &\quad [\bar{s}\gamma^\mu P_L b] [\bar{e}_a \gamma_\mu (|[U_L]_{4a}|^2 P_L + |[U_R]_{4a}|^2 P_R) e_a]. \end{aligned}$$

Hence, the contributions of this diagram to the Wilson coefficients are

$$\begin{aligned} C_9^{\text{NP(a)}} &= -\frac{1}{s_W^2} \frac{1}{4} (|[U_L]_{4a}|^2 + |[U_R]_{4a}|^2) g_1(x_i, y), \\ C_{10}^{\text{NP(a)}} &= \frac{1}{s_W^2} \frac{1}{4} (|[U_L]_{4a}|^2 - |[U_R]_{4a}|^2) g_1(x_i, y). \end{aligned} \tag{47}$$

**Diagram (b)**

$$\begin{aligned} \square^{(b)} &= \left(\frac{g}{\sqrt{2}}\right)^4 \sum_{i=u,c,t} V_{ib} V_{is}^* \int \frac{d^4 q}{(2\pi)^4} \left(\frac{-i}{q^2 - M_W^2}\right)^2 \left[ \bar{s}\gamma^\mu P_L \frac{i(\not{q} + M_i)}{q^2 - M_i^2} \frac{M_i}{M_W} P_L b \right] \\ &\quad \left[ \bar{e}_a \frac{-v([Y^{\nu L} U_R^*]_{4a} P_L + [Y^{\nu R} U_L^*]_{4a} P_R)}{M_W} \frac{i(\not{q} + M_L)}{q^2 - M_L^2} (|[U_L]_{4a}\gamma_\mu P_L + [U_R]_{4a}\gamma_\nu P_R) e_a \right] \\ &= \frac{g^4}{4} \sum_{i=u,c,t} V_{ib} V_{is}^* \int \frac{d^4 q}{(2\pi)^4} \frac{1}{(q^2 - M_W^2)^2 (q^2 - M_i^2) (q^2 - M_L^2)} \\ &\quad \left[ \bar{s}\gamma^\mu P_L (\not{q} + M_i) \frac{M_i}{M_W} P_L b \right] \\ &\quad \left[ \bar{e}_a \frac{-v([Y^{\nu L} U_R^*]_{4a} P_L + [Y^{\nu R} U_L^*]_{4a} P_R)}{M_W} (\not{q} + M_L) (|[U_L]_{4a}\gamma_\mu P_L + [U_R]_{4a}\gamma_\nu P_R) e_a \right]. \end{aligned}$$

The last two square brackets can be written as

$$-\frac{vM_i^2M_L}{M_W^2}[\bar{s}\gamma^\mu P_L b][\bar{e}_a\gamma_\mu([U_L]_{4a}[Y^{\nu R^*}U_L^*]_{4a}P_L + [U_R]_{4a}[Y^{\nu L^*}U_R^*]_{4a}P_R)e_a],$$

where we have dropped terms linear in  $q$ . Using Eq. 44,

$$\begin{aligned} \square^{(b)} = & -\frac{g^4}{4} \sum_{i=u,c,t} V_{ib}V_{is}^* B(M_i, M_L) \frac{vM_i^2M_L}{M_W^2} [\bar{s}\gamma^\mu P_L b] \\ & [\bar{e}_a\gamma_\mu([U_L]_{4a}[Y^{\nu R^*}U_L^*]_{4a}P_L + [U_R]_{4a}[Y^{\nu L^*}U_R^*]_{4a}P_R)e_a]. \end{aligned}$$

Putting all these together, we have

$$\begin{aligned} \square^{(b)} = & i\frac{4G_F}{\sqrt{2}} \sum_{i=u,c,t} V_{ib}V_{is}^* \frac{e^2}{16\pi^2} \frac{1}{s_W^2} \frac{1}{2} \frac{v}{M_L} x_i y g_0(x_i, y) \\ & [\bar{s}\gamma^\mu P_L b][\bar{e}_a\gamma_\mu([U_L]_{4a}[Y^{\nu R^*}U_L^*]_{4a}P_L + [U_R]_{4a}[Y^{\nu L^*}U_R^*]_{4a}P_R)e_a]. \end{aligned}$$

Hence, the contributions of this diagram to the Wilson coefficients are

$$\begin{aligned} C_9^{\text{NP}(b)} &= \frac{1}{s_W^2} \frac{1}{4} \frac{v}{M_L} x_i y ([U_L]_{4a}[Y^{\nu R^*}U_L^*]_{4a} + [U_R]_{4a}[Y^{\nu L^*}U_R^*]_{4a}) g_0(x_i, y), \\ C_{10}^{\text{NP}(b)} &= -\frac{1}{s_W^2} \frac{1}{4} \frac{v}{M_L} x_i y ([U_L]_{4a}[Y^{\nu R^*}U_L^*]_{4a} - [U_R]_{4a}[Y^{\nu L^*}U_R^*]_{4a}) g_0(x_i, y). \end{aligned} \tag{48}$$

**Diagram (c)**

$$\begin{aligned} \square^{(c)} &= \left(\frac{g}{\sqrt{2}}\right)^4 \sum_{i=u,c,t} V_{ib}V_{is}^* \int \frac{d^4q}{(2\pi)^4} \left(\frac{-i}{p^2 - M_W^2}\right)^2 \left[ \bar{s} \frac{M_i}{M_W} P_R \frac{i(\not{q} + M_i)}{q^2 - M_i^2} \gamma^\mu P_L b \right] \\ & \left[ \bar{e}_a([U_L^*]_{4a}\gamma_\mu P_L + [U_R^*]_{4a}\gamma_\mu P_R) \frac{i(\not{q} + M_L) - v([Y^{\nu L}U_R]_{4a}P_R + [Y^{\nu R}U_L]_{4a}P_L)}{q^2 - M_L^2} \frac{1}{M_W} e_a \right] \\ &= \frac{g^2}{4} \sum_{i=u,c,t} V_{ib}V_{is}^* \int \frac{d^4q}{(2\pi)^4} \frac{1}{(q^2 - M_W^2)^2 (q^2 - M_i^2) (q^2 - M_L^2)} \\ & \left[ \bar{s} \frac{M_i}{M_W} P_R (\not{q} + M_i) \gamma^\mu P_L b \right] \\ & \left[ \bar{e}_a([U_L^*]_{4a}\gamma_\mu P_L + [U_R^*]_{4a}\gamma_\mu P_R) (\not{q} + M_L) \frac{-v([Y^{\nu L}U_R]_{4a}P_R + [Y^{\nu R}U_L]_{4a}P_L)}{M_W} e_a \right]. \end{aligned}$$

The last two square brackets can be written as

$$-\frac{vM_i^2M_L}{M_W^2}[\bar{s}\gamma^\mu P_L b][\bar{e}_a\gamma_\mu([U_L^*]_{4a}[Y^{\nu R}U_L]_{4a}P_L + [U_R^*]_{4a}[Y^{\nu L}U_R]_{4a}P_R)e_a],$$

where we have dropped terms linear in  $q$ . Using Eq. 44,

$$\begin{aligned} \square^{(c)} = & -\frac{g^4}{4} \sum_{i=u,c,t} V_{ib} V_{is}^* B(M_i, M_L) \frac{v M_i^2 M_L}{M_W^2} [\bar{s} \gamma^\mu P_L b] \\ & [\bar{e}_a \gamma_\mu ([U_L^*]_{4a} [Y^{\nu R} U_L]_{4a} P_L + [U_R^*]_{4a} [Y^{\nu L} U_R]_{4a} P_R) e_a]. \end{aligned}$$

Putting all these together, we have

$$\begin{aligned} \square^{(c)} = & i \frac{4G_F}{\sqrt{2}} \sum_{i=u,c,t} V_{ib} V_{is}^* \frac{e^2}{16\pi^2} \frac{1}{s_W^2} \frac{1}{2} \frac{v}{M_L} x_i y g_0(x_i, y) \\ & [\bar{s} \gamma^\mu P_L b] [\bar{e}_a \gamma_\mu ([U_L^*]_{4a} [Y^{\nu R} U_L]_{4a} P_L + [U_R^*]_{4a} [Y^{\nu L} U_R]_{4a} P_R) e_a]. \end{aligned}$$

Hence, the contributions of this diagram to the Wilson coefficients are

$$\begin{aligned} C_9^{\text{NP}(c)} &= \frac{1}{s_W^2} \frac{1}{4} \frac{v}{M_L} x_i y ([U_L^*]_{4a} [Y^{\nu R} U_L]_{4a} + [U_R^*]_{4a} [Y^{\nu L} U_R]_{4a}) g_0(x_i, y), \\ C_{10}^{\text{NP}(c)} &= -\frac{1}{s_W^2} \frac{1}{4} \frac{v}{M_L} x_i y ([U_L^*]_{4a} [Y^{\nu R} U_L]_{4a} - [U_R^*]_{4a} [Y^{\nu L} U_R]_{4a}) g_0(x_i, y). \end{aligned} \quad (49)$$

**Diagram (d)**

$$\begin{aligned} \square^{(d)} &= \left( \frac{g}{\sqrt{2}} \right)^4 \sum_{i=u,c,t} V_{ib} V_{is}^* \int \frac{d^4 q}{(2\pi)^4} \left( \frac{-i}{q^2 - M_W^2} \right)^2 \left[ \bar{s} \frac{M_i}{M_W} P_R \frac{i(\not{q} + M_i)}{q^2 - M_i^2} \frac{M_i}{M_W} P_L b \right] \\ & \left[ \bar{e}_a \frac{v([Y^{\nu L} U_R^*]_{4a} P_L + [Y^{\nu R} U_L^*]_{4a} P_R)}{M_W} \frac{i(\not{q} + M_L)}{q^2 - M_L^2} \right. \\ & \left. \frac{v([Y^{\nu L} U_R]_{4a} P_R + [Y^{\nu R} U_L]_{4a} P_L)}{M_W} e_a \right] \\ &= \frac{g^4}{4} \sum_{i=u,c,t} V_{ib} V_{is}^* \int \frac{d^4 q}{(2\pi)^4} \frac{1}{(q^2 - M_W^2)(q^2 - M_i^2)(q^2 - M_L^2)} \\ & \left[ \bar{s} \frac{M_i}{M_W} P_R (\not{q} + M_i) \frac{M_i}{M_W} P_L b \right] \left[ \bar{e}_a \frac{v([Y^{\nu L} U_R^*]_{4a} P_L + [Y^{\nu R} U_L^*]_{4a} P_R)}{M_W} \right. \\ & \left. (\not{q} + M_L) \frac{v([Y^{\nu L} U_R]_{4a} P_R + [Y^{\nu R} U_L]_{4a} P_L)}{M_W} e_a \right]. \end{aligned}$$

The last two square brackets can be written as

$$q_\alpha q_\beta \frac{v^2 M_i^2}{M_W^4} [\bar{s} \gamma^\alpha P_L b] [\bar{e}_a \gamma^\beta (|[Y^{\nu R} U_L]_{4a}|^2 P_L + |[Y^{\nu L} U_R]_{4a}|^2 P_R) e_a],$$

where we have dropped terms linear in  $q$ . Using Eq. 43,

$$\begin{aligned} \square^{(d)} &= \frac{g^4}{4} \sum_{i=u,c,t} V_{ib} V_{is}^* A_{\alpha\beta}(M_i, M_L) \frac{v^2 M_i^2}{M_W^4} [\bar{s} \gamma^\alpha P_L b] \\ & [\bar{e}_a \gamma^\beta (|[Y^{\nu R} U_L]_{4a}|^2 P_L + |[Y^{\nu L} U_R]_{4a}|^2 P_R) e_a]. \end{aligned}$$

Putting all these together, we have

$$\begin{aligned} \square^{(d)} = & -i \frac{4G_F}{\sqrt{2}} \sum_{i=u,c,t} V_{ib} V_{is}^* \frac{e^2}{16\pi^2} \frac{1}{s_W^2} \frac{1}{8} \frac{v^2}{M_L^2} x_i y g_1(x_i, y) \\ & [\bar{s} \gamma^\mu P_L b] [\bar{e}_a \gamma_\mu (|[Y^{\nu R} U_L]_{4a}|^2 P_L + |[Y^{\nu L} U_R]_{4a}|^2 P_R) e_a]. \end{aligned}$$

Hence, the contributions of this diagram to the Wilson coefficients are

$$\begin{aligned} C_9^{\text{NP(d)}} &= -\frac{1}{s_W^2} \frac{1}{16} \frac{v^2}{M_L^2} x_i y (|[Y^{\nu R} U_L]_{4a}|^2 + |[Y^{\nu L} U_R]_{4a}|^2) g_1(x_i, y), \\ C_{10}^{\text{NP(d)}} &= \frac{1}{s_W^2} \frac{1}{16} \frac{v^2}{M_L^2} x_i y (|[Y^{\nu R} U_L]_{4a}|^2 - |[Y^{\nu L} U_R]_{4a}|^2) g_1(x_i, y). \end{aligned} \quad (50)$$

### Total Contributions

The sum of the Wilson coefficients from these four diagrams (Eq. 47 - Eq. 50) is the total NP Wilson coefficients,

$$\begin{aligned} C_9^{\text{NP}} &= -\frac{1}{s_W^2} \frac{1}{4} [U_1^+(x, y) g_1(x, y) + U_0^+(x, y) g_0(x, y)], \\ C_{10}^{\text{NP}} &= \frac{1}{s_W^2} \frac{1}{4} [U_1^-(x, y) g_1(x, y) + U_0^-(x, y) g_0(x, y)], \end{aligned} \quad (51)$$

where  $x = M_t^2/M_W^2$ ,  $y = M_L^2/M_W^2$ ,

$$g_1(x, y) = \frac{1}{x-y} \left[ \frac{x^2}{(x-1)^2} \log x - \frac{y^2}{(y-1)^2} \log y - \frac{1}{x-1} + \frac{1}{y-1} \right], \quad (52)$$

$$g_0(x, y) = \frac{1}{x-y} \left[ \frac{x}{(x-1)^2} \log x - \frac{y}{(y-1)^2} \log y - \frac{1}{x-1} + \frac{1}{y-1} \right], \quad (53)$$

and

$$U_1^\pm(x, y) = |[U_L]_{4a}|^2 \pm |[U_R]_{4a}|^2 + \frac{1}{4} \frac{v^2}{M_L^2} x y \left( |[Y^{\nu R} U_L]_{4a}|^2 \pm |[Y^{\nu L} U_R]_{4a}|^2 \right), \quad (54)$$

$$\begin{aligned} U_0^\pm(x, y) = & -\frac{v}{M_L} x y \left( [U_L]_{4a} [Y^{\nu R*} U_L^*]_{4a} + [U_L^*]_{4a} [Y^{\nu R} U_L]_{4a} \right. \\ & \left. \pm [U_R]_{4a} [Y^{\nu L*} U_R^*]_{4a} \pm [U_R^*]_{4a} [Y^{\nu L} U_R]_{4a} \right). \end{aligned} \quad (55)$$

## References

- [1] **Particle Data Group** Collaboration, C. Patrignani *et al.*, “Review of Particle Physics,” *Chin. Phys.* **C40** (2016), no. 10, 100001.
- [2] R. Dermíšek and A. Raval, “Explanation of the Muon  $g-2$  Anomaly with Vectorlike Leptons and its Implications for Higgs Decays,” *Phys. Rev.* **D88** (2013) 013017, 1305.3522.
- [3] F. del Aguila, J. de Blas, and M. Perez-Victoria, “Effects of new leptons in Electroweak Precision Data,” *Phys. Rev.* **D78** (2008) 013010, 0803.4008.
- [4] A. Joglekar, P. Schwaller, and C. E. M. Wagner, “Dark Matter and Enhanced Higgs to Di-photon Rate from Vector-like Leptons,” *JHEP* **12** (2012) 064, 1207.4235.
- [5] J. Kearney, A. Pierce, and N. Weiner, “Vectorlike Fermions and Higgs Couplings,” *Phys. Rev.* **D86** (2012) 113005, 1207.7062.
- [6] K. Ishiwata and M. B. Wise, “Phenomenology of heavy vectorlike leptons,” *Phys. Rev.* **D88** (2013), no. 5, 055009, 1307.1112.
- [7] A. J. Buras and M. Munz, “Effective Hamiltonian for  $B \rightarrow X_s e^+ e^-$  beyond leading logarithms in the NDR and HV schemes,” *Phys. Rev.* **D52** (1995) 186–195, hep-ph/9501281.
- [8] C. Bobeth, M. Misiak, and J. Urban, “Photonic penguins at two loops and  $m_t$  dependence of  $BR[B \rightarrow X_s l^+ l^-]$ ,” *Nucl. Phys.* **B574** (2000) 291–330, hep-ph/9910220.
- [9] T. Inami and C. S. Lim, “Effects of Superheavy Quarks and Leptons in Low-Energy Weak Processes  $k_L \rightarrow \mu \bar{\mu}$ ,  $K^+ \rightarrow \pi^+ \nu \bar{\nu}$  and  $K^0 \leftrightarrow \bar{K}^0$ ,” *Prog. Theor. Phys.* **65** (1981) 297. [Erratum: *Prog. Theor. Phys.* 65,1772(1981)].
- [10] **LHCb** Collaboration, R. Aaij *et al.*, “Test of lepton universality using  $B^+ \rightarrow K^+ \ell^+ \ell^-$  decays,” *Phys. Rev. Lett.* **113** (2014) 151601, 1406.6482.
- [11] **LHCb** Collaboration, R. Aaij *et al.*, “Test of lepton universality with  $B^0 \rightarrow K^{*0} \ell^+ \ell^-$  decays,” 1705.05802.
- [12] A. Falkowski, D. M. Straub, and A. Vicente, “Vector-like leptons: Higgs decays and collider phenomenology,” *JHEP* **05** (2014) 092, 1312.5329.

- [13] S. A. R. Ellis, R. M. Godbole, S. Gopalakrishna, and J. D. Wells, “Survey of vector-like fermion extensions of the Standard Model and their phenomenological implications,” *JHEP* **09** (2014) 130, 1404.4398.
- [14] R. Dermisek, J. P. Hall, E. Lunghi, and S. Shin, “Limits on Vectorlike Leptons from Searches for Anomalous Production of Multi-Lepton Events,” *JHEP* **12** (2014) 013, 1408.3123.
- [15] N. Kumar and S. P. Martin, “Vectorlike leptons at the Large Hadron Collider,” *Phys. Rev.* **D92** (2015), no. 11, 115018, 1510.03456.
- [16] L. Lavoura, “General formulae for  $f_1 \rightarrow f_2 \gamma$ ,” *Eur. Phys. J.* **C29** (2003) 191–195, hep-ph/0302221.
- [17] A. Djouadi, “The Anatomy of electro-weak symmetry breaking. I: The Higgs boson in the standard model,” *Phys. Rept.* **457** (2008) 1–216, hep-ph/0503172.
- [18] D. Straub, P. Stangl, Christoph Niehoff, E. Gurler, J. Kumar, sreicher, and F. Beaujean, “flav-io/flavio v0.21.1,” Apr., 2017.
- [19] **Muon g-2** Collaboration, A. Chapelain, “The Muon g-2 experiment at Fermilab,” *EPJ Web Conf.* **137** (2017) 08001, 1701.02807.
- [20] A. K. Alok, B. Bhattacharya, A. Datta, D. Kumar, J. Kumar, and D. London, “New Physics in  $b \rightarrow s \mu^+ \mu^-$  after the Measurement of  $R_{K^*}$ ,” 1704.07397.
- [21] H. H. Patel, “Package-X: A Mathematica package for the analytic calculation of one-loop integrals,” *Comput. Phys. Commun.* **197** (2015) 276–290, 1503.01469.